JOURNAL OF OPTOELECTRONICS AND ADVANCED MATERIALS Vol. 9, No. 3, March 2007, p. 702 - 707

Analysis of band structure and electric field in two-dimensional surface plasmon-polariton crystals

E. VINȚELER*, S. AȘTILEAN
Physics Department, Univ. Babeş-Bolyai, M. Kogalniceanu 1, 400084 Cluj-Napoca, Romania

The behavior of electric field in two-dimensional surface-plasmon polaritonic crystals is presented. First the photonic band structure for surface plasmon-polariton propagating across the square lattice of metal (silver) hemi-ellipsoids is calculated by using the two-dimensional reduced Rayleigh equation. Then we calculated the normalized electric field E_z at mid-distance between hemi-ellipsoids for two high-symmetry points X and M in the first Brillouin zone and found out the regions of highest electric field, which are of great interest for understanding the electromagnetic mechanism in surface-enhanced Raman scattering.

(Received November 15, 2006; accepted December 21, 2006)

Keywords: Photonic crystals, Photonic band gap, Surface plasmons, Reduced Rayleigh equation

1. Introduction

In recent years the optical properties of materials that possess a periodic modulation of their refraction index on the scale of the wavelength of light have received much attention [1, 2]. Such materials can exhibit *photonic band gaps* that are very much like the *electronic band gaps* for electron waves traveling in the periodic potential of a crystal. In both cases frequency intervals exist where wave propagation is forbidden. Materials with band gaps for propagation of light waves are called *photonic crystals* [3]. The existence of *photonic band gaps* allows complete control over the radiative dynamics of atoms and molecules embedded in photonic crystals such as the inhibition of spontaneous emission for transition frequencies [4-6].

A special case of photonic crystals are the periodic metallic nanostructures which support electromagnetic excitations called surface plasmon-polariton (SPP) modes. The SPP are evanescent waves produced by the resonant interaction between light and free electrons at the interface of metallic and dielectric materials. The excitation of surface plasmons in plasmon-polariton crystals can play a crucial role in light-matter interactions too [7, 8]. For instance, intensive gathering of the surface plasmon modes on nanostructured metallic surface gives rise to high density of states and local field enhancements. These features find various applications in optical data storage, miniaturized photonic circuits, surface-enhanced Raman scattering, biosensing, light generation, and solar cells [9].

In recent years, a great deal of effort has been devoted to study the properties of plasmonic crystals both theoretically and experimentally [10-13]. The aim of this work is to calculate the band structure of SPPs for a square lattice of metal (silver) hemi-ellipsoids deposited on a flat metallic surface and determine the regions of highest electric field and highest density of electromagnetic modes between hemi-ellipsoids [12, 13]. Our study is of great interest for understanding the mechanism of enhancing Raman signal (SERS) from molecules adsorbed on such metallic nanostructures. Resonant interaction of light with surface plasmon polaritons [14-16] and interference of diffracted evanescent waves more recently [17], are the main mechanisms proposed for the enhanced transmission in Surface Plasmon Resonance (SPR) and Surface Enhanced Raman Scattering (SERS).

2. Theory of two-dimensional reduced Rayleigh equation

We consider a double periodic rough interface separating a metal (silver) medium in the region $x_3<\zeta(\mathbf{x}_{\|})$ and a vacuum in the region $x_3>\zeta(\mathbf{x}_{\|})$, where $\mathbf{x}_{\|}=(x_1, x_2, 0)$ (see Fig. 1). The profile function that describes a square lattice of hemi-ellipsoids with radius R and height HR can be written in the form:

$$\zeta(\mathbf{x}_{\|}) = \sum_{m} S(\mathbf{x}_{\|} - \mathbf{x}_{\|}^{(m)}), \qquad (1a)$$

where

$$S(\mathbf{x}_{\|}) = \begin{cases} H\sqrt{R^2 - x_{\|}^2}, & |\mathbf{x}_{\|}| \le R \\ 0, & |\mathbf{x}_{\|}| > R \end{cases} \qquad (1b)$$

Its Fourier series representation admits an analytic form [12]:

$$\xi^{(\mathbf{m})}(\gamma) = \begin{cases} 1 + \dfrac{2\pi R^2}{a_c} \displaystyle\sum_{n=1}^{\infty} \dfrac{(\gamma HR)^n}{n!\,(n+2)} & \mathbf{m} = 0 \\ \dfrac{2\pi R^2}{a_c} \displaystyle\sum_{n=1}^{\infty} \dfrac{(\gamma HR)^n}{n!} \dfrac{2^{n/2}\,\Gamma(n/2+1)}{(G_{\parallel}^{(\mathbf{m})} R)^{n/2+1}} J_{n/2+1}(G_{\parallel}^{(\mathbf{m})} R) & \mathbf{m} \neq 0 \end{cases} \quad (2)$$

where J and Γ are the Bessel function of the first kind and respectively gamma function.

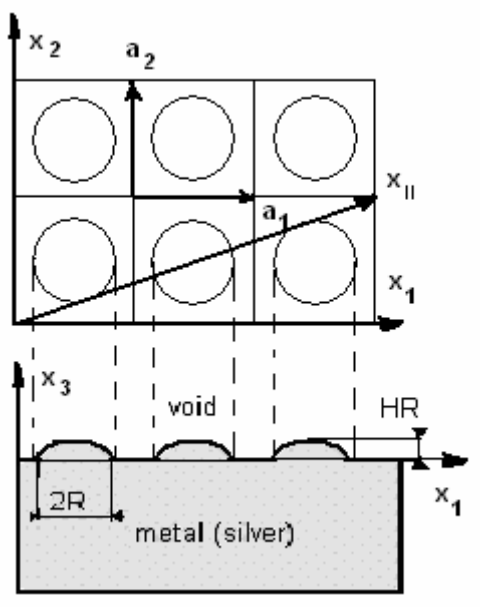

Fig. 1. Double-periodic square lattice. Up: View from above of square lattice with primitive translation vectors a_1 and a_2. Down: Cross-section of hemi - ellipsoids with radius R and height HR.

The position of each unit cell of the square lattice describing the periodic array of scatterers is given by: $\mathbf{x}_{\parallel}^{(\mathbf{m})} = m_1\,\mathbf{a_1} + m_2\,\mathbf{a_2}$, where $\mathbf{a_1}$, $\mathbf{a_2}$ are the primitive vectors of the (square) lattice, while m_1 and m_2 are two integers labeling the unit cells, collectively denoted by **m**. The position of cells within the associated reciprocal lattice are defined by $\mathbf{G}_{\parallel}^{(\mathbf{m})} = m_1\,\mathbf{b_1} + m_2\,\mathbf{b_2}$, where $\mathbf{b_1}$, $\mathbf{b_2}$ are the primitive vectors of the reciprocal-lattice satisfying the relation $\mathbf{a_i} \cdot \mathbf{b_j} = 2\pi\,\delta_{ij}$, I,j=1,2. The primitive vectors of the square lattice and its reciprocal-lattice are: $\mathbf{a_1} = a(1,0)$, $\mathbf{a_2} = a\,(0,1)$, $\mathbf{b_1} = 2\pi/a\,(1,0)$, $\mathbf{b_2} = 2\pi/a\,(0,1)$. The area of each unit cell is $a_c = |\,\mathbf{a_1} \times \mathbf{a_2}|$ and for square lattice $a_c = 1$.

The electric field in the vacuum can be written in the form:

$$\mathbf{E}(\mathbf{x}, t) = \sum_{\mathbf{m}} \exp(i\,\mathbf{K}_{\parallel}^{(\mathbf{m})} \cdot \mathbf{x}_{\parallel} - \beta_0^{(\mathbf{m})} x_3 - i\,\omega\,t) \times$$
$$\times \left\{ \frac{c}{\omega} [\,i\,\hat{\mathbf{K}}_{\parallel}^{(\mathbf{m})} \beta_0^{(\mathbf{m})} - \hat{\mathbf{x}}_3 K_{\parallel}^{(\mathbf{m})}]\, A_p^{(\mathbf{m})}(\mathbf{k}_{\parallel}) + [\hat{\mathbf{x}}_3 \times \hat{\mathbf{K}}_{\parallel}^{(\mathbf{m})}]\, A_s^{(\mathbf{m})}(\mathbf{k}_{\parallel}) \right\} \quad (3)$$

where $\mathbf{k}_{\parallel} = (k_1, k_2, 0)$ is the wave-vector of SPP. We use abbreviations: $\mathbf{K}_{\parallel}^{(\mathbf{m})} = \mathbf{k}_{\parallel} + \mathbf{G}_{\parallel}^{(\mathbf{m})}$, $K_{\parallel}^{(\mathbf{m})} = |\mathbf{K}_{\parallel}^{(\mathbf{m})}|$, $\hat{\mathbf{K}}_{\parallel}^{(\mathbf{m})} = \mathbf{K}_{\parallel}^{(\mathbf{m})} / K_{\parallel}^{(\mathbf{m})}$. We define the function:

$$\beta_0^{(\mathbf{m})} = [(\,\mathbf{K}_{\parallel}^{(\mathbf{m})})^2 - (\omega/c)^2]^{1/2} \quad (4)$$

The subscripts s and p of the coefficients $A_s^{(\mathbf{m})}$ and $A_p^{(\mathbf{m})}$ denote the s-polarized, respectively p-polarized components of the electric field with respect to the direction of propagation. These coefficients satisfy the homogenous form of two-dimensional reduced Rayleigh equations that has the following form [18]:

$$\sum_{nm} \frac{\xi^{(n-m)}(\beta^{(n)} - \beta_0^{(m)})}{\beta^{(n)} - \beta_0^{(m)}} \begin{bmatrix} \mathbf{K}_{\parallel}^{(n)} \mathbf{K}_{\parallel}^{(m)} - \beta^{(n)} (\hat{\mathbf{K}}_{\parallel}^{(m)} \cdot \hat{\mathbf{K}}_{\parallel}^{(m)}) \beta_0^{(m)} & -\frac{i\omega}{c} \beta^{(n)} (\hat{\mathbf{K}}_{\parallel}^{(n)} \times \hat{\mathbf{K}}_{\parallel}^{(m)})_3 \\ \frac{i\omega}{c} \beta_0^{(m)} (\hat{\mathbf{K}}_{\parallel}^{(n)} \times \hat{\mathbf{K}}_{\parallel}^{(m)})_3 & (\frac{\omega}{c})^2 (\hat{\mathbf{K}}_{\parallel}^{(m)} \cdot \hat{\mathbf{K}}_{\parallel}^{(m)}) \end{bmatrix} \begin{bmatrix} A_p^{(m)}(\mathbf{k}_{\parallel}) \\ A_s^{(m)}(\mathbf{k}_{\parallel}) \end{bmatrix} = 0 \quad (5)$$

The (2×2) matrix in eq. (5) couples the two different polarization modes. This nonperturbative approach, based on reduced Rayleigh equation, is valid for any rough dielectric substrate that support SPPs. Eq.(5) is exact within the domain of validity of the Rayleigh hypothesis, which can be defined by the condition for profile function $|\nabla\,\zeta(x_{\parallel})| << 1$ [18]. In our case, the profile function given by eq. (1) is non-analytic and violates the Rayleigh hypothesis. However, it was shown in papers [19,20] that convergent results can be obtained if the hemi-ellipsoids are not too high $H \leq 0.4$ and the number of Fourier coefficients $\xi^{(\mathbf{m})}(\gamma)$ is limited. In this way is obtained an analytic profile function that approximates the initial profile function and for which the Rayleigh hypothesis is valid.

We have defined the following function:

$$\beta^{(\mathbf{m})} = [(\,\mathbf{K}_{\parallel}^{(\mathbf{m})})^2 - \varepsilon(\omega)\,(\omega/c)^2]^{1/2} \quad (6)$$

The functions $\beta_0^{(\mathbf{m})}$ and $\beta^{(\mathbf{m})}$ are the inverse decay lengths of the electromagnetic field of a surface polariton into the vacuum, respectively into the medium (in the case where $K_{\parallel}^{(\mathbf{m})} > \omega/c$).

The medium is characterized by a real, isotropic, frequency-dependent dielectric function ε(ω). Dielectric function is described within Drude nearly free-electron model:

$$\varepsilon(\omega) = 1 - \omega_p^2 / \omega^2 \quad (7)$$

where ω_p is the plasma frequency of conduction electron in the bulk of the metal. The polaritons considered here are surface-plasmon polaritons associated with collective oscillations of the surface electron density. We require that $\mathrm{Re}(\varepsilon(\omega)) < -1$ in some frequency range. It is within this frequency range that surface polaritons exist, when $\omega < (1/\sqrt{2})\,\omega_p$. For silver we have the value $\hbar\,\omega_p = 3.78$ eV.

3. Method of calculation

We present dispersion curves, density-of-states and electric field for non-radiative modes without ohmic losses. They are calculated for wave vectors $\mathbf{k}_{\parallel}=(k_1,k_2,0)$

along the boundary of the irreducible part of the first Brillouin zone of the square lattice. Without ohmic losses and for real ω, we have a real, negative dielectric constant ε(ω) in the frequency range in which surface-plasmon can exist, in other words when $0 \le \omega < \omega_p$. In this region $\beta_0^{(\mathbf{m})}$ is purely real for wave vectors with $k_1^2 + k_2^2 > (\omega/c)^2$, and $\beta^{(\mathbf{m})}$ is purely real for all wave vectors $\mathbf{k}_\parallel$ within the irreducible element of the first Brillouin zone. These modes define Bloch-type surface-plasmon polaritons that are true eigenmodes of the system. They occur within the non-radiative region of the $(\omega, \mathbf{k}_\parallel)$ space.

In order to solve numerically the dispersion relation from eq. (5) we had to truncate the infinite summations by restricting the number of reciprocal-lattice vectors $\mathbf{G}_\parallel^{(\mathbf{m})} = m_1\,\mathbf{b_1} + m_2\,\mathbf{b_2}$ to those satisfying $m_1^2 + m_2^2 \le N_{max}^2$. The calculation was done with $N_{max}=12$ or equivalently 441 reciprocal lattice vectors, which leads to (882 × 882) matrix (the number is doubled due to the two polarizations modes).

The solution of dispersion relation is based on the search for real zeros of a real-valued determinant. For a fixed $\mathbf{k}_\parallel$, we sampled the interval $(0, \omega_p)$ for sign changes of the determinant, and classified the frequencies at which these occurred in the order of increased magnitude. This collection constitutes the different branches of the dispersion curve.

The convergence was achieved when the relative deviation δ between two dispersion relations was smaller than 1%:

$$\delta = \frac{1}{n_b n_k} \sum_{\text{branches}} \sum_{k\parallel} \frac{|\,\omega_a(\mathbf{k}_\parallel) - \omega_b(\mathbf{k}_\parallel)\,|}{|\,\omega_a(\mathbf{k}_\parallel)\,|}, \qquad (8)$$

where $\omega_a(\mathbf{k}_\parallel)$ and $\omega_b(\mathbf{k}_\parallel)$ are calculated for N_{max}, respectively $N_{max}+1$ and n_b is the number of branches and n_k is the number of wave vectors.

The density of states is defined as a sum over all wave vectors in the first Brillouin zone and the sum over the real parts of the different frequency branches.

$$\sigma(\omega) = \sum_{\text{branches}} \sum_{k\parallel} \delta(\omega - \mathrm{Re}\,\omega(k_\parallel)), \qquad (9)$$

The electric field is non-zero only along dispersion curves and is computed using eq. (3) in terms of the coefficients $A_s^{(\mathbf{m})}$ and $A_p^{(\mathbf{m})}$. These coefficients are calculated from the system of homogenous equations (5). Due to the fact that the determinant of the (882 × 882) matrix eq. (5) is null along dispersion curves and its rank is 880 there exist a certain freedom in choosing the solutions. The two-dimensional reduced Rayleigh equations are obtained from Maxwell equations at metal-vacuum interface [18] and we know that the solutions of Maxwell equations are not unique, but are defined up to a term characterizing gauge freedom. In two dimensions we must impose exactly 2 conditions to fix this gauge freedom. For the two-dimensional reduced Rayleigh equations we can do this by fixing the two coefficients $A_s^{(\mathbf{m0})}=1$ and $A_p^{(\mathbf{m0})}=1$ (where $\mathbf{m0}=(m_1,m_2)=(0,0)$), express all the other coefficients in terms of these two and obtain the electric field. Of course we can fix other transformati and the electric field obtained will be related with the previous one by a two-dimensional gauge transformation.

The convergence for the z-component of electric field was achieved when the relative deviation δ_p for a given point $\mathbf{k}_\parallel$ on two dispersion relations was smaller than 1%:

$$\delta_p = \frac{1}{n_m} \sum_{\mathbf{m}} \frac{|\,A_{p,a}^{(\mathbf{m})}(\mathbf{k}_\parallel) - A_{p,b}^{(\mathbf{m})}(\mathbf{k}_\parallel)\,|}{|\,A_{p,a}^{(\mathbf{m})}(\mathbf{k}_\parallel)\,|}, \qquad (10)$$

where $A_{p,a}^{(\mathbf{m})}$ and $A_{p,b}^{(\mathbf{m})}$ are calculated for N_{max}, respectively $N_{max}+1$ and $n_m = 441$ is the number of coefficients $A_p^{(\mathbf{m})}$. (The z-component of electric field depends only of the coefficients $A_p^{(\mathbf{m})}$).

4. Results

In order to define the band gap in the photonic spectrum of non-radiative modes for surface plasmon-polariton propagating across the square lattice of hemi-ellipsoids we calculated the dispersion relations along the boundary of the irreducible part of the first Brillouin zone. To confirm that the frequencies within the occurring gap are truly inhibited for any wave vector we plot the density of states as given by eq. (9).

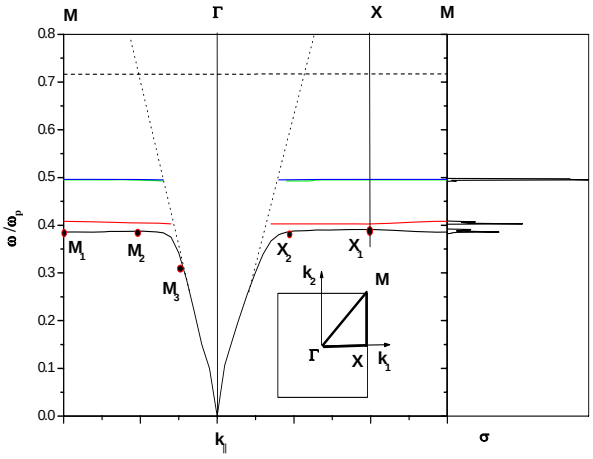

Fig. 2. Dispersion curves and density of states for square lattice. Left: Non-radiative modes of the first four lowest frequency branches are plotted as functions of $\mathbf{k}_\parallel$ in the irreducible part of the first Brillouin zone (plotted in the inset). Right: Density of states as a function of ω/ω_p in arbitrary units.

In Fig. 2 the non-radiative modes of the first four lowest frequency branches are plotted as functions of $\mathbf{k}_\parallel$ and the density of states as a function of ω/ω_p. The third and fourth branch have nearly the same values.

The inset in the figure displays the first Brillouin zone with its irreducible part and the high-symmetry points

Γ=(0,0), X= π/a (1,0) and M= π/a (1,1). The parameters used in obtaining this plot are: a=147 nm, R=70 nm, H=0.4. The height of hemi-ellipsoids H was chosen to its maximal possible value for which calculations still converge in order to get the maximum interaction of the SPP and the surface. The calculation was done with N_{max} =12 or equivalently 441 reciprocal lattice vectors, which leads to (882 × 882) matrix.

The dotted line represents the light line $\omega = c\, k_{\|}$ and the dashed line represents the surface plasmon frequency $\omega=\omega_p/\sqrt{2}$. We have two band gaps for the non-radiative modes: the first is a narrow gap between ω_1= 0.391ω_p= 1.478 eV and ω_2 =0.403 ω_p= 1.523 eV; the second is a large gap between ω_3= 0.408ω_p= 1.542 eV and ω_4 =0.493 ω_p= 1.863 eV. It is within this frequency range that the density of states vanishes.

We represent six special points that are located on the first branch on line ΓM: M_1 = π/a (1,1), M_2 = π/a (1/2,1/2) M_3 = π/a (1/4,1/4) and on line ΓX: X_1 = π/a (1,0), X_2 = π/a (1/2,0). The points M_1 and X_1 are different from the points M and X because the frequency is restricted: ω (M_1) = 0.386ω_p and ω (X_1) = 0.391ω_p. This is also true for the other special points. We are interested in the behavior of electric field (at mid-distance between hemi-ellipsoids) in these special points when we change the distance between the hemi-ellipsoids. In Fig. 3 and Fig. 4 we plot the electric field for the points M_1, M_2, M_3, respectively the points X_1, X_2. In Fig. 5 and 6 we choose only the point M_1 and look at the electric field at two fixed distances between the hemi-ellipsoids d=7 nm and respectively d=45 nm.

In Fig. 3 is plotted the z-component of the normalized electric field E_z /E_{z0} at mid-distance between hemi-ellipsoids as a function of the distance *d* between the margins of hemi-ellipsoids (d = a – 2R). E_{z0} is the electric field at distance *d*=160 nm between the margins of hemi-ellipsoids. Black line, red line and blue line corresponds to M_1 point, M_2 point, and respectively M_3 point (see Fig. 2). The parameters are: R=70 nm, H=0.4 and N_{max}=12. We observe that the electric field has an oscillatory behavior with peaks of decreasing heights (when we increase the distance between hemi-ellipsoids). The electric field also decrease when we decrease the impulse of SPP, in other words when we pass from the curve M_1 to M_2 and from M_2 to M_3. For all three curves the highest peak of normalized electric field is at the distance of d=7 nm. Two special points A and B on the curve corresponding to M_1 point indicate two distances d=7nm and d=45 nm when the normalized electric field is 17.02, and respectively 2.43. These points appear also in the center of Fig. 4 and Fig. 5 indicating the normalized electric field at mid-distance between hemi-ellipsoids.

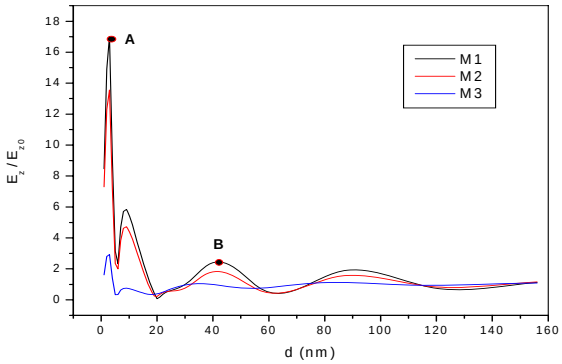

Fig. 3. Normalized electric field at mid-distance between hemi-ellipsoids as a function of the distance d between the margins of hemi-ellipsoids in Brillouin point M.

In Fig. 4 is plotted the z-component of the normalized electric field E_z /E_{z0} at mid-distance between hemi-ellipsoids as a function of the distance *d* between the margins of hemi-ellipsoids. E_{z0} is the electric field at distance *d*=160 nm between the margins of hemi-ellipsoids. Black line and red line corresponds to X_1 point and respectively X_2 point (see Fig. 2). The parameters are: R=70 nm, H=0.4 and N_{max}=12.

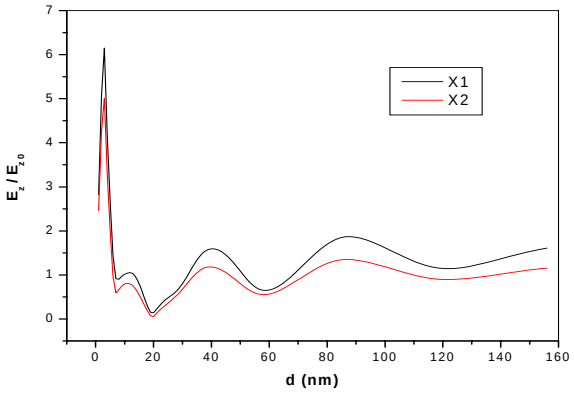

Fig. 4. Normalized electric field at mid-distance between hemi-ellipsoids as a function of the distance d between the margins of hemi-ellipsoids in Brillouin point X.

When we compare Fig. 4 with Fig. 3 we observe the same oscillatory behavior of the electric field with peaks of decreasing heights (when we increase the distance between hemi-ellipsoids) and also the decreasing of the electric field when we decrease the impulse of SPP (when we pass from the curve X_1 to X_2). The form of curves for the electric field also depends on the state of polarization as can be seen by comparing Fig. 4 with Fig. 3.

In Fig. 5 is plotted a section through the normalized electric field E_z /E_{z0} as function of the distance x. The centers of hemi-ellipsoids are at x = 0 nm and x = 147 nm. The distance between the margins of hemi-ellipsoids is d = 7 nm (the gap between hemi-ellipsoids begins at x=70 nm

and ends at x= 77 nm). We observe that the electric field in point A has the highest value of 17.02 at the mid-distance between hemi-ellipsoids (x = 73.5 nm). The parameters are: a=147 nm, R=70 nm, H=0.4 and N_{max} =12.

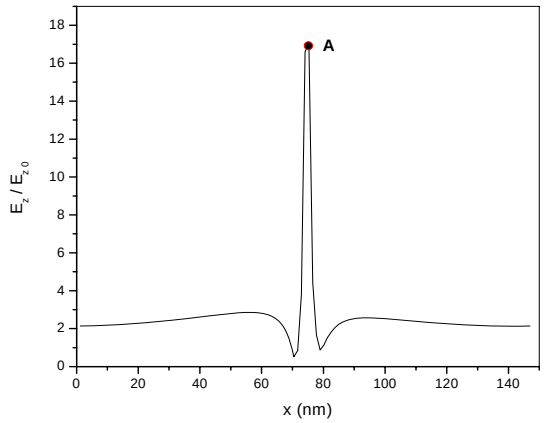

Fig. 5. Normalized electric field at d=7 nm as a function of the distance x from the center of hemi-ellipsoid.

In Fig. 6 is plotted a section through the normalized electric field E_z / E_{z0} as function of the distance x. The centers of hemi-ellipsoids are at x = 0 nm and x = 185 nm. The distance between the margins of hemi-ellipsoids is d = 45 nm (the gap between hemi-ellipsoids begins at x=70 nm and ends at x= 115 nm). We observe that the electric field has the highest value of 3.86 near the margins of hemi-ellipsoids at x= 74.9 and x=113.1 nm. The electric field in point B has a value of only 2.43 at the mid-distance between hemi-ellipsoids (x = 92.5 nm). The parameters are: a=185 nm, R=70 nm, H=0.4 and N_{max} =12.

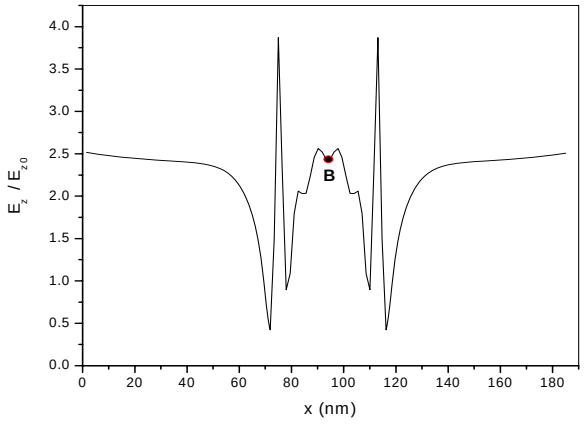

Fig. 6. Normalized electric field at d=45 nm as a function of the distance x from the center of hemi-ellipsoid.

5. Conclusions

The plots of normalized electric field for two high-symmetry points X and M of the first Brillouin zone (Fig. 3,4) show an oscillatory character. Periodic oscillations can be noticed at specific frequencies in the points M_1, M_2 and X_1 , X_2 just under the first band gap. The periodic behavior is evidence of a mutual exchange of energy between two or more beams inside the crystals. This effect is a well known phenomenon, extensively studied for X-ray or neutron diffraction in ordinary crystals. The same phenomenon has been recently studied in two-dimensional photonic crystals [21] and three-dimensional opal photonic crystals [22] as an effect related to negative refraction. Fig. 1 and 2 show the excitation of a single SPP mode with a small imaginary part leading to a damping of the oscillations that increases when we depart from the frequency of the first band gap (when we pass from M_1, M_2 to M_3 and from X_1 to X_2) .

For small distance between the margins hemi-ellipsoids Fig. 5 shows a normal, expected behavior of electric field with the highest value at the mid-distance between hemi-ellipsoids. But for big distance between the margins hemi-ellipsoids Fig. 6 shows that the region of highest value of electric field is just near the margins where the slope of surface is highest. The determination of regions of highest value of electric field is important for SERS and can be verified experimentally through the enhancement of Raman signals of molecules adsorbed on metallic surfaces, in particular on noble metal films deposited over colloidal crystals [23-25].

References

[1] E. Yablonovitch, Phys. Rev. Lett. **58**, 2059 (1987).
[2] S. John, Phys. Rev. Lett. **58**, 2486 (1987).
[3] K. Sakoda, Optical properties of photonic crystals, Springer, (2001).
[4] J. D. Joannopoulos, R. D. Meade, J. N. Winn, Photonic Crystals, Princeton University Press, Princeton, NJ, (1995).
[5] S. G. Johnson, J. D. Joannopoulos, Photonic Crystals: The Road from Theory to Practice, Kluwer, Boston, (2002).
[6] J. Martorell, N. M Lawandy, Phys Rev Lett. **65**, 1877-1880 (1990).
[7] W. L. Barnes, A. Dereux, T. W. Ebbesen, Nature **424**, 824 (2003).
[8] J. B. Pendry, L. Martín-Moreno, F. J. Garcia-Vidal, Science **305**, 847 (2004).
[9] S. A. Maier, P. G. Kik, H. A. Atwater, S. Meltzer, E. Harel, B. E.Koel, A. A. G. Requicha, Nat. Mater. **2**, 229 (2003).
[10] S. I. Bozhevolyi, J. Erland, K. Leosson, P. M. W. Skovgaard, J. M. Hvam, Phys. Rev. Lett. **86**, 3008 (2001).
[11] W. L. Barnes, S. C. Kitson, T. W. Preist, J. R. Sambles, J. Opt. Soc. Am. A **14**, 1654 (1997)
[12] M. Kretschmann, A. A. Maradudin, Phys. Rev. **B66**, 245408 (2002).

[13] M. Kretschmann, Phys. Rev. **B68**, 125419 (2003).
[14] D. E. Grupp, H. J. Lezec, T. W. Ebbesen, K. M. Pellerin, T. Thio, Appl. Phys. Lett. **77**, 1569 (2000).
[15] Q-j. Wang, J-q. Li, C-p. Huang, C. Zhang, Y-y. Zhu, Appl. Phys. Lett. **87**, 091105 (2005).
[16] W. L. Barnes, W. A. Murray, J. Dintinger, E. Devaux, T. W. Ebbesen, Phys. Rev. Lett. **92**, 107401 (2004).
[17] H. J. Lezec, T. Thio, Opt. Express **12**, 3629 (2004).
[18] G. C. Brown, V. Celli, M. Haller, A. Marvin, Surf. Sci. **136**, 381 (1984).
[19] B. Laks, D. L. Mills, A. A. Maradudin, Phys. Rev. B **23**, 4965 (1981).
[20] N. E. Glass, A. A. Maradudin, J. Opt. Soc. Am. **73**, 1240 (1983).
[21] V. Mocella, Opt. Express **13**, 1361 (2005).
[22] A. Balestreri, L. C. Andreani, M. Agio, Phys. Rev. E **74**, 036603 (2006).
[23] M. Baia, L. Baia, J. Popp, S. Astilean, Appl Phys Lett. **88**, 143121 (2006).
[24] M. Baia, L. Baia, S. Astilean, Chem. Phys. Lett. **404**, 3 (2005).
[25] S. Astilean, Radiation Physics and Chemistry (in press, 2006).

*Corresponding author: evinteler@phys.ubbcluj.ro